


Pore-Network Modeling of Solute Transport and Biofilm Growth in Porous Media

Chao-Zhong Qin¹  · S. Majid Hassanizadeh¹

Received: 22 March 2015 / Accepted: 6 July 2015 / Published online: 5 September 2015
© The Author(s) 2015. This article is published with open access at Springerlink.com

Abstract In this work, a pore-network (PN) model for solute transport and biofilm growth in porous media was developed. Compared to previous studies of biofilm growth, it has two new features. First, the constructed pore network gives a better representation of a porous medium. Second, instead of using a constant mass exchange coefficient for solute transport between water phase and biofilm, a variable coefficient as a function of biofilm volume fraction and Damköhler number was employed. This PN model was verified against direction simulations. Then, a number of case studies were conducted, in order to illustrate the temporal evolutions of medium permeability and biomass content under different operating conditions. Finally, we explored the effects of biofilm morphology and permeability on biofilm growth, as well as non-unique relationship between medium permeability reduction and its porosity change.

Keywords Pore-network (PN) modeling · Biofilm growth and clogging · Permeability reduction · Non-equilibrium mass exchange · Numerical simulation

1 Introduction

In many natural and engineered porous media, biofilm may present under both saturated and unsaturated conditions. When nutrients are continuously available, biofilm keeps growing on solid walls. This would finally lead to the condition of bioclogging in porous media (Baveye et al. 1998; Pintelon et al. 2009). Up to now, there have been many applications by using biofilm such as biobarriers, microbial-enhanced oil recovery (Afrapoli et al. 2011), and bioremediation. In wastewater treatment, biofilm plays a major role in biological aerated filters for removing carbon and nitrogen (Boltz et al. 2010). In in situ bioremediation, biofilm breaks down contaminants into less toxic or non-toxic substances (Cunningham and Mendoza-Sanchez 2006). In subsurface CO₂ storage, engineered biofilm is used to plug CO₂

✉ Chao-Zhong Qin
c.qin@uu.nl; chaozhong.qin@gmail.com

¹ Department of Earth Sciences, Faculty of Geosciences, University of Utrecht,
Budapestlaan 4, P. O. Box 80021, 3584 CD Utrecht, The Netherlands

leakage pathways (Ebigbo et al. 2010; Mitchell et al. 2009). Also, biofilm plays an important role in inhibiting the corrosion process of metallic structures such as sheet piles and oil pipes (Potekhina et al. 1999; Videla and Herrera 2009; Zuo 2007).

Much effort has been invested into understanding biodegradation and bioclogging in porous media (Baveye and Valocchi 1989; Dillon and Fauci 2000; Kapellos et al. 2007; Rittmann 1993; Rosenzweig et al. 2009; Taylor et al. 1990; Van Noorden et al. 2010). To describe these processes at the REV scale, macroscale models were formulated by the volume-averaging technique (Taylor and Jaffe 1990; Vandevivere et al. 1995). In such models, a number of effective parameters are commonly needed, which are determined by the pore-scale information. For tracking solute transport in porous media with biofilm, one-equation models have been developed under both equilibrium and non-equilibrium conditions. Then, effective parameters such as dispersivity and effectiveness factor (representing the observed reaction rate versus the maximal reaction rate) were obtained by solving pore-scale closure problems (Davit et al. 2010; Golfier et al. 2009; Orgogozo et al. 2010). Also, Cunningham and Mendoza-Sanchez (2006) mathematically determined the conditions under which a simple one-equation model was equivalent to a complex biofilm model (MarDonald et al. 1999). Alternatively, under non-equilibrium conditions, a two-equation model was widely used (e.g., Cherblanc et al. 2007; Ebigbo et al. 2010, 2012). In this approach, two transport equations of solute in water phase and biofilm are coupled by an empirical first-order kinetic model. But, it is difficult to characterize the mass exchange coefficient appearing in the kinetic mass exchange model (see Dykaar and Kitanidis 1996; Qin and Hassanizadeh 2015). Therefore, an assumed constant mass exchange coefficient has been used in most previous studies (e.g., Ebigbo et al. 2010, 2012; Kim and Corapcioglu 1997; Thullner et al. 2002; Zysset et al. 1994). To release this assumption, a reliable and efficient pore-scale model needs to be developed, which is the main objective of this work.

For obtaining constitutive equations for macroscale models and gaining insights into flow and transport processes in porous media with biofilm, pore-scale studies have received much attention (e.g., Dupin et al. 2001; Pintelon et al. 2012; Suchomel et al. 1998a, b; Xu et al. 2011). Fabricated micromodels were used to study biomass evolution and its effect on permeability (e.g., Cunningham et al. 1991; Dunsmore et al. 2004; Kim and Fogler 2000). Recently, Iltis et al. (2011) visualized 3D biofilm structures in a glass bead pack using synchrotron-based X-ray computed microtomography. In numerical studies, several pore-scale models have been widely used, such as pore-network (PN) model and Lattice–Boltzmann (LB) model. Graf von der Schulenburg et al. (2009) developed a LB model for biofilm growth in porous media, in which biofilm evolution was tracked by an individual-based biofilm model (IBM). Later, Pintelon et al. (2012) further developed the LB model to study the effect of biofilm permeability on bioclogging. Bottero et al. (2013) conducted 2D direct simulations of biofilm growth and the dynamics of preferential flow paths in porous media. However, it is worth noting that these direct simulations including LB modeling are computationally expensive.

PN models have been extensively used in modeling flow and transport in porous media (Blunt 2001; Budek and Szymczak 2012; Li et al. 2006; Raoof et al. 2012). There are also many studies of bioclogging using PN models. Kim and Fogler (2000) developed a PN model for tracking biofilm evolution under starvation conditions. They showed that with a proper critical shear stress, simulations were in qualitative agreement with the experimental results. Thullner et al. (2002) developed a 2D lattice-based PN model for predicting the relationship between biomass content and permeability of porous medium. Later, Thullner and Baveye (2008) extended the 2D model to a 3D regular lattice-based PN model. They showed that biofilm permeability had a large impact on the temporal evolution and distribution pattern of

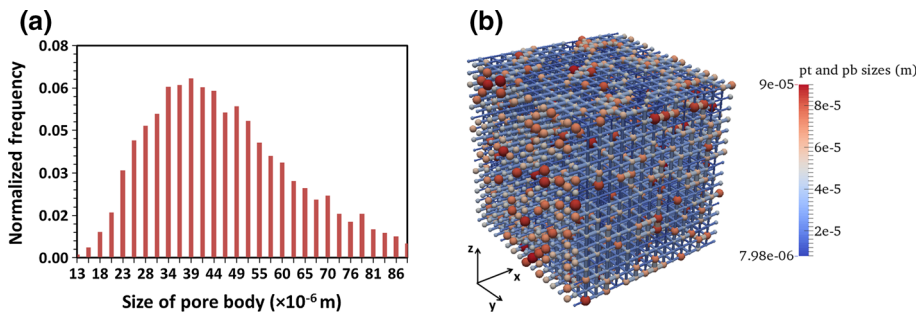


Fig. 1 **a** Distribution of the pore-body sizes in the pore network; **b** the generated $16 \times 16 \times 16$ pore network colored according to the pore size

biofilm. Recently, [Ezeuko et al. \(2011\)](#) developed a PN model with a so-called dual-diffusion mass exchange model.

Despite these advances, there exist several deficiencies with previous PN models of biofilm growth. First, a porous medium has been usually simplified by a network of cylindrical tubes connected by volumeless nodes. Second, either a constant mass exchange coefficient or mass-equilibrium assumption has been employed (e.g., [Thullner and Baveye 2008](#); [Ezeuko et al. 2011](#)). This assumption would give rise to an incorrect prediction of the temporal evolution of biofilm under non-equilibrium conditions. The main objective of this work is to develop a PN model for solute transport in porous media and the associated biofilm growth, which is devoid of the two above-mentioned deficiencies.

2 Pore-Network Generation

Many geological and industrial porous media can be adequately represented by a network of pore bodies and throats. Usually, pore bodies of proper shapes are used to represent large pore spaces in a porous medium, while pore throats are used to represent narrow regions which connect two neighboring pore bodies. Pore throats are the main contributors to flow resistance, particularly in the case of saturated flow. In the literature, there have been several approaches to generating a pore network which needs to be calibrated in terms of material properties such as porosity, permeability, capillary pressure curve, and pore size and coordinate number distributions. This can be applied to a regular lattice-based network or a stochastically generated network ([Raoof and Hassanizadeh 2010](#); [Jiang et al. 2012](#)). Furthermore, a more realistic pore network may be directly extracted from micro-CT images of a porous medium ([Al-Kharusi and Blunt 2007](#)).

In this work, with the purpose of a general study of solute transport and biofilm growth, a regular lattice-based pore network was generated to represent the representative elementary volume (REV) of sandstone. The pore-body size is approximated by a truncated lognormal distribution ([Al-Kharusi and Blunt 2007](#)) as shown in Fig. 1a. The size of a pore throat is determined by the smaller connected pore body by assuming a constant aspect ratio (AR) of the pore-throat radius to the pore-body radius (see Sect. 3.3).

Figure 1b shows the generated $16 \times 16 \times 16$ pore network colored according to the sizes of pore bodies and throats. Each pore body has a coordinate number of six, except for those at inlet, outlet, and side boundaries. For saturated flow in porous media, the pore shape distribution is not as important as in unsaturated flow in which corner flow plays an important

Table 1 Geometric information of the generated pore network

Pore network overall dimensions	$0.003 \times 0.003 \times 0.003$ m
Numbers of pore bodies and pore throats	4096/10,560
Lattice distance (l)	2.0×10^{-4} m
Porosity (ε)	0.17
Permeability (K^0)	1.38×10^{-11} m ²
Minimum and maximum sizes of pore body	$1.0 \times 10^{-5}/9.0 \times 10^{-5}$ m
Mean size of pore body	4.5×10^{-5} m

role. But, it does have some effect on the distribution pattern of biofilm (Qin and Hassanizadeh 2015). In this work, for simplicity, we used spherical pore bodies and cylindrical pore throats. The detailed information of the generated pore network is given in Table 1. Finally, it is noted that the developed PN model is in a general form. Its governing equations do not depend on the used network structure. A more realistic network structure will be considered in further studies.

3 Pore-Network Model

3.1 Main Assumptions

The following main assumptions have been made in the development of the present PN model:

1. Saturated water flow is considered.
2. Detached biomass does not influence water flow.
3. Planktonic biomass in water phase and attachment of biomass onto biofilm are neglected.
4. The biofilm growth is controlled by a rate-limiting solute.
5. Homogenous biofilm grows uniformly around the solid walls in pore bodies and/or pore throats.

3.2 Governing Equations

Governing equations are formulated in terms of pore-body-averaged and pore-throat-averaged quantities. We adopt the classic approximation that the time scale of biofilm growth is much larger than the time scale associated with transport and consumption of solute (Orgogozo et al. 2010). As a result, we can decouple solute transport and biofilm growth. Note that in the following, we assume that the biofilm permeability is so low that water flow through biofilm can be neglected.

3.2.1 Flow Field

Average water pressure is assigned to each pore body. Flow resistance of the network is assumed to be caused by pore throats only. In each pore throat, the steady-state water flux is calculated by Hagen–Poiseuille equation (see Fig. 2). At pore body i , the water volume conservation is given as

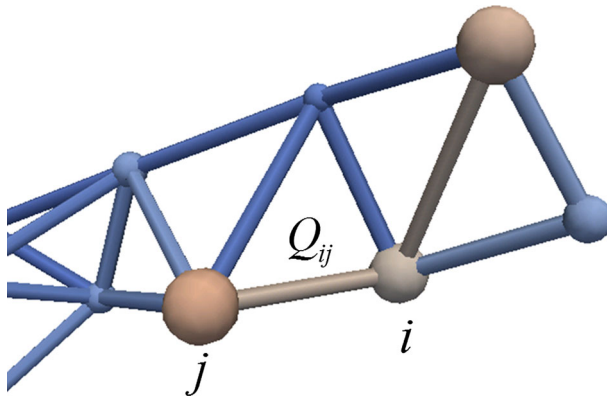


Fig. 2 Schematic representation of a pore network connectivity

$$\sum_j^{N_i} Q_{ij} = \sum_j^{N_i} G_{ij} \frac{(p_i - p_j)}{L_{ij}} = 0 \quad (1)$$

where the index j denotes a neighboring pore body, N_i is the coordinate number of pore body i , Q_{ij} [L^3/T] is the volumetric flow rate of water from pore body i to j , G_{ij} [L^5T/M] is the conductivity of pore throat ij , L_{ij} is the length of pore throat, and p [M/LT^2] is the water pressure at pore body.

3.2.2 Transport of a Rate-Limiting Solute

For modeling solute transport in the pore network, average concentrations of solute are assigned to water phase and biofilm at pore bodies and throats. Transport processes including advection, dispersion, and mass exchange between water phase and biofilm, as well as bioreaction in biofilm, are taken in account. It is assumed that the consumption of solute in biofilm can be modeled with Monod-type kinetics (Cunningham and Mendoza-Sanchez 2006).

For a rate-limiting solute, the mass conservations in water phase and biofilm in pore body i can be given, respectively, as

$$\begin{aligned} V_i^0 \varepsilon_i^w \frac{dC_i^w}{dt} = & -C_i^w \sum_j^{N_i} \max(Q_{ij}, 0) - \sum_j^{N_i} C_{ij}^w \min(Q_{ij}, 0) - \sum_j^{N_i} D_{ij}^w A_{ij}^w \frac{C_i^w - C_{ij}^w}{L_{ij}/2} \\ & - V_i^0 \frac{D_w D_b}{D_w + D_b} \gamma_i \xi_i (C_i^w - C_i^b) \end{aligned} \quad (2)$$

$$\begin{aligned} V_i^0 \varepsilon_i^b \frac{dC_i^b}{dt} = & - \sum_j^{N_i} D_b A_{ij}^b \frac{C_i^b - C_{ij}^b}{L_{ij}/2} + V_i^0 \frac{D_w D_b}{D_w + D_b} \gamma_i \xi_i (C_i^w - C_i^b) \\ & - V_i^0 \varepsilon_i^b k \frac{C_i^b}{K_s + C_i^b} \rho_b \end{aligned} \quad (3)$$

where the superscripts w and b refer to the water phase and biofilm, respectively, V_i^0 [L^3] is the volume of pore body i in the absence of biofilm, ε_i^w and ε_i^b are the volume fractions of water phase and biofilm, respectively, subject to the restriction $\varepsilon_i^w + \varepsilon_i^b = 1$, C [M/L^3] is the

average mass concentration of solute, D_{ij} [L^2/T] is the dispersion coefficient for transport in the pore throat ij , A_{ij}^w [L^2] is the cross-sectional area for water flow, A_{ij}^b is the cross-sectional area occupied by biofilm, D_w and D_b [L^2/T] are the molecular diffusivities of solute in the water phase and biofilm, respectively, γ_i [$1/L$] is the specific surface area of biofilm in the pore body, ξ_i [$1/L$] is the mass exchange coefficient between water phase and biofilm, k [$1/T$] is the maximum bioreaction rate, K_s [M/L^3] is the half-saturation constant, and ρ_b [M/L^3] is the biomass density. In Eq. 2, the l.h.s denotes the temporal accumulation of solute in the water phase; the first and second terms on the r.h.s denote the advective fluxes of solute out of pore body i and into pore body i from the surrounding pore throats, respectively; the third term on the r.h.s. represents the dispersive mass flux exchanged between pore body i and its surrounding pore throats in the water phase; and the last term represents the flux of solute diffusing into the biofilm. The formula for the latter term was obtained by [Qin and Hassanizadeh \(2015\)](#), who also developed equations for dependence of ξ_i on biofilm volume fraction and Damköhler number. In Eq. 3, the l.h.s denotes the temporal accumulation of solute in the biofilm; on the r.h.s., the first term denotes the dispersive mass flux between pore body i and its surrounding pore throats within the biofilm, the second term is the flux of solute diffusing from the water phase, and the last term represents the rate of solute consumption due to bioreaction.

Similarly, the mass conservation equations of solute in water phase and biofilm in pore throat ij can be written as

$$V_{ij}^0 \varepsilon_{ij}^w \frac{dC_{ij}^w}{dt} = (C_i^w - C_{ij}^w) \max(Q_{ij}, 0) + (C_{ij}^w - C_j^w) \min(Q_{ij}, 0) + D_{ij}^w A_{ij}^w \frac{C_i^w - C_{ij}^w}{L_{ij}/2} + D_{ij}^w A_{ij}^w \frac{C_j^w - C_{ij}^w}{L_{ij}/2} - V_{ij}^0 \frac{D_w D_b}{D_w + D_b} \gamma_{ij} \xi_{ij} (C_{ij}^w - C_{ij}^b) \quad (4)$$

$$V_{ij}^0 \varepsilon_{ij}^b \frac{dC_{ij}^b}{dt} = D_b A_{ij}^b \frac{C_i^b - C_{ij}^b}{L_{ij}} + D_b A_{ij}^b \frac{C_j^b - C_{ij}^b}{L_{ij}} + V_{ij}^0 \frac{D_w D_b}{D_w + D_b} \gamma_{ij} \xi_{ij} (C_{ij}^w - C_{ij}^b) - V_{ij}^0 \varepsilon_{ij}^b k \frac{C_{ij}^b}{K_s + C_{ij}^b} \rho_b \quad (5)$$

where V_{ij}^0 is the volume of pore throat ij in the absence of biofilm, ε_{ij}^w and ε_{ij}^b are the volume fractions of water phase and biofilm, respectively, subject to $\varepsilon_{ij}^w + \varepsilon_{ij}^b = 1$.

3.2.3 Biofilm Growth

Biofilm evolution with time in the pore network is primarily controlled by the growth, decay, and detachment of biofilm ([Vandevivere et al. 1995](#)). Once solute concentrations in pore bodies and pore throats are obtained, biofilm volume fractions are updated using the following two equations

$$\rho_b V_i^0 \frac{d\varepsilon_i^b}{dt} = \rho_b V_i^0 \varepsilon_i^b k Y \frac{C_i^b}{K_s + C_i^b} - \rho_b V_i^0 \varepsilon_i^b \mu_{\text{decay}} \quad (6)$$

$$\rho_b V_{ij}^0 \frac{d\varepsilon_{ij}^b}{dt} = \rho_b V_{ij}^0 \varepsilon_{ij}^b k Y \frac{C_{ij}^b}{K_s + C_{ij}^b} - \rho_b \varepsilon_{ij}^b V_{ij}^0 \mu_{\text{decay}} - r_{ij}^{\text{det}} \quad (7)$$

where Y is the yield coefficient accounting for the fraction of solute actually used for biofilm growth, μ_{decay} [$1/T$] is the decay rate of biofilm, and r_{ij}^{det} [$M/L^3 T$] is the detached biomass

mainly due to the water shear force. Note that the detachment is neglected in pore bodies due to relatively small water shear force there.

3.3 Auxiliary Equations

The conductivity of a pore throat for water flow that was introduced in Eq. 1 may change with time due to biofilm growth. For cylindrical pores, the following equation can be obtained

$$G_{ij} = \frac{\pi (r_{ij}^0)^4}{8\mu} (1 - \varepsilon_{ij}^b)^2 \quad (8)$$

where μ [M/LT] is the dynamic viscosity of water and r_{ij}^0 [L] is the radius of pore throat ij in the absence of biofilm. The length of pore throat ij is calculated as $L_{ij} = l - r_i^0 - r_j^0$, and its radius is determined by $r_{ij}^0 = 0.7 \times \min(r_i^0, r_j^0)$. The volumes of pore body i and pore throat ij are, respectively, given as $V_i^0 = 4\pi (r_i^0)^3/3$ and $V_{ij}^0 = \pi (r_{ij}^0)^2 L_{ij}$. The cross-sectional areas for water flow and biofilm are, respectively, calculated as $A_{ij}^w = \pi (r_{ij}^0)^2 (1 - \varepsilon_{ij}^b)$ and $A_{ij}^b = \pi (r_{ij}^0)^2 \varepsilon_{ij}^b$. The specific surface areas of biofilm in pore body i and pore throat ij are calculated, respectively, as $\gamma_i = 3(1 - \varepsilon_i^b)^{2/3}/r_i^0$ and $\gamma_{ij} = 2(1 - \varepsilon_{ij}^b)^{1/2}/r_{ij}^0$. In pore throat ij , when the water shear force on the biofilm exceeds a critical value τ_c , the biofilm starts to be detached (Chambless and Steward 2007; Stewart and Kim 2004). The rate of biomass detachment is assumed to be proportional to the water shear force such that the sink term r_{det} is given as

$$r_{ij}^{\text{det}} = V_{ij}^0 \rho_b \mu_{\text{det}} (1 - \varepsilon_{ij}^b) \frac{Q_{ij}}{K_{ij}} \text{ when } r_{ij}^0 \sqrt{1 - \varepsilon^b} |p_i - p_j| / 2L_{ij} > \tau_c \quad (9)$$

where μ_{det} (1/T) is the detachment rate. It is worth noting that biomass detachment is a complicated process which is mainly in the form of erosion or sloughing. For more detail, one can refer to the Introduction in Pintelon et al. (2009).

In pore throat ij , the dispersivity of solute in the water phase is approximated by Taylor–Aris dispersion formula (Aris 1956)

$$D_{ij}^w = D_w \left(1 + \frac{Pe^2}{192} \right) \quad (10)$$

where $Pe = 2Q_{ij}/\pi r_{ij}^0 \sqrt{1 - \varepsilon^b} D_w$ is Péclet number for water flow in the pore throat.

Finally, we need to provide constitutive equations for the mass exchange coefficients ξ_i and ξ_{ij} , appearing in Eqs. (2–5), which depend on a number of variables, such as biofilm volume fraction and Damköhler number. More detail is given in the next subsection.

3.4 Mass Exchange Coefficient ξ

Most recently, Qin and Hassanizadeh (2015) studied the mass exchange of a solute between water phase and biofilm in a single pore. The aim of that study was to investigate the relationship between mass exchange rate and prevailing conditions. Results were upscaled for a single pore in order to obtain the tube-scale mass exchange coefficients. It was found that the coefficient depends on Damköhler number, $Da = k\rho_b (2r_{ij}^0)^2 / K_s D_w$, biofilm volume

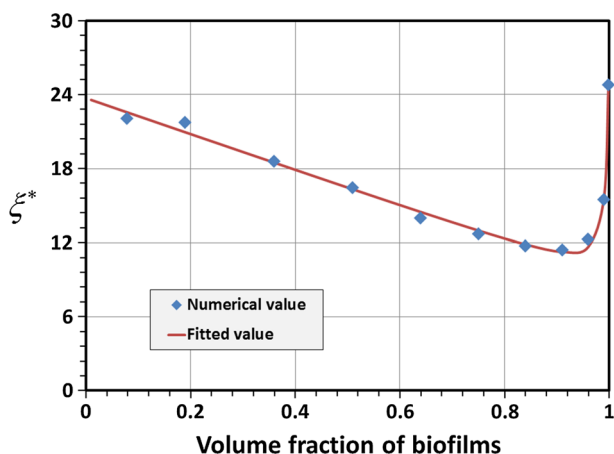


Fig. 3 Dependency of the dimensionless mass exchange coefficient on biofilm volume fraction when zeroth-order bioreaction is considered

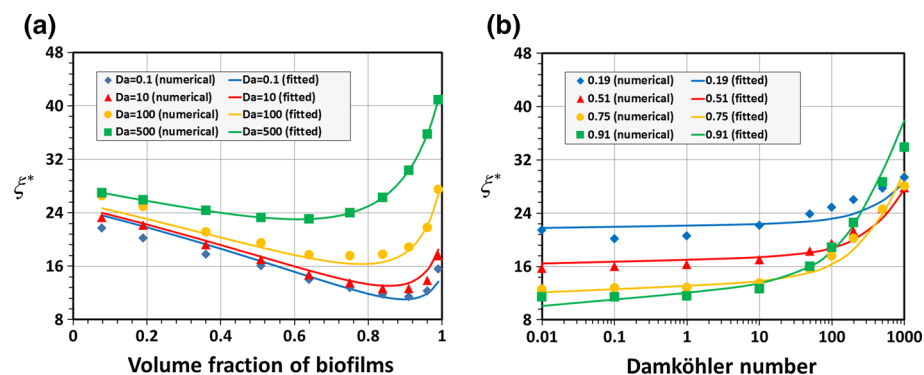


Fig. 4 Dependencies of the dimensionless mass exchange coefficient on biofilm volume fraction and Damköhler number when first-order bioreaction is considered

fraction, ε^b , dimensionless inlet solute concentration, C_{in}^* , and diffusivity ratio, $\Gamma = D_b/D_w$. These dependences are intricately coupled.

First, we fixed the diffusivity ratio to be 0.5 and considered high solute concentrations such that Monod kinetics reduced to zeroth-order reaction. It was found that the dimensionless mass exchange coefficient $\xi_{ij}^* = 2r_{ij}^0/\xi_{ij}$ could be well described as a function of biofilm volume fraction. As shown in Fig. 3, ξ_{ij}^* decreases with the decrease in biofilm volume fraction, except at extremely high biofilm volume fractions where it increases sharply. The fitted expression of ξ_{ij}^* is given as

$$\xi_{ij}^* = \frac{-9.7 \times 10^{-2} \varepsilon_{ij}^b}{\varepsilon_{ij}^b - 1.0} - 14.7 \varepsilon_{ij}^b + 23.7 \quad (11)$$

Next, we kept the diffusivity ratio to be 0.5, but considered low solute concentrations such that Monod kinetics reduced to first-order reaction. It was found that ξ_{ij}^* depended on biofilm volume fraction and Damköhler number as shown in Fig. 4a, b. The fitted formula for ξ_{ij}^* is given as

$$\xi_{ij}^* = \frac{-52.2 + 6.23 \times 10^{-2} \ln(Da) + 18.2 \exp(\varepsilon_{ij}^b)}{1 + 1.63 \times 10^{-4} Da - 0.94 \varepsilon_{ij}^b} + 58.9 \quad (12)$$

Finally, it is assumed that the dimensionless mass exchange coefficient ξ_i has the same functional forms as Eqs. 11 and 12, with the Damköhler number in pore body i being defined as $Da = k\rho_b (2r_i^0)^2 / K_s D_w$.

4 Description of Numerical Simulations

In Sect. 3.1, we have presented governing Eqs. (1–5) for a rate-limiting solute transport in the pore network when considering impermeable biofilm. For permeable biofilm, governing equations are given in detail in Appendix 1. To solve solute transport in the pore network, a general numerical scheme presented in Appendix 2 was used. The employed boundary conditions are as follows. For water flow, constant pressure values were assigned to the inlet and outlet pore bodies, respectively. For solving concentrations, a constant inlet solute concentration in the water was assumed. The diffusive flux and the flux of solute within biofilm at both inlet and outlet boundaries were set to zero. Finally, we employed the following initial conditions. Zero solute concentrations were assumed everywhere in the pore network, and an initial biofilm volume fraction of $\varepsilon_{\text{ini}} = 0.01$ was set, in order to support subsequent biofilm growth.

In this work, in order to investigate a rate-limiting solute transport associated with the biofilm growth under different operating conditions, a number of case studies have been conducted. First, we verified the developed PN model against direct simulation. In the verification study, we used a one-dimensional pore network as shown in Fig. 5. It has fifty pore bodies connected by forty-nine pore throats. Biofilm is assumed to be distributed only in the pore throats with a constant volume fraction of 0.75. The size of pore bodies was randomly selected between 10^{-5} and 9×10^{-5} m. The size of pore throat was determined by its two connected pore bodies. The employed geometric and physical parameters are listed in Table 2. In the direct simulation, we discretized the pore space into computational grids and solved the 2D axisymmetric advection-diffusion-reaction equation. This was done in the commercial software COMSOL. Note that during both PN and direct simulations, the biofilm volume fraction did not evolve with time. The verification was in terms of pressure drop and steady-state solute concentration distributions along the network.

For the purpose of this work, six cases were selected for PN simulations. They are described in Table 3. Case 1 was set to be the base case with the employed physical parameters listed in Table 4. In the base case study, we assumed that impermeable biofilm only existed in pore

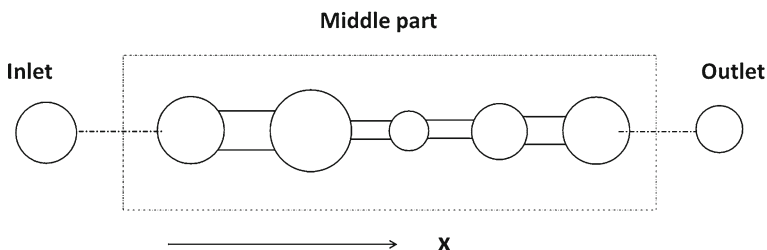


Fig. 5 Schematic representation of the pore network used in the verification study

Table 2 Parameters used in verification study

Parameter	Value + units
Domain length	1.225×10^{-2} m
Lattice distance (l)	2.5×10^{-4} m
Numbers of pore bodies and pore throats	50/49
Pressure drop (Δp)	3000 Pa
Maximum reaction rate (k)	1.6×10^{-3} 1/s
Half-saturation constant (K_s)	2.0×10^{-3} kg/m ³
Solute diffusivity in biofilm (D_b)	5.0×10^{-10} m ² /s
Solute diffusivity in water (D_w)	1.0×10^{-9} m ² /s
Biofilm density (ρ_b)	2.0 kg/m ³
Inlet solute concentration (C_{in})	1.0×10^{-4} kg/m ³

Table 3 List of the case studies associated with parameter settings

Case number	Parameter settings
Case 1	Base case
Case 2	$\Delta p = 50$ Pa
Case 3	$C_{in} = 1.0$ kg/m ³
Case 4	$C_{in} = 0.1$ kg/m ³
Case 5	Biofilm in pore bodies and pore throats
Case 6	Permeable biofilm in pore bodies and pore throats

Table 4 Physical parameters for the base case study

Parameter	Value + units
Decay rate of biofilm (μ_{decay})	1.0×10^{-6} 1/s
Detachment rate of biofilm (μ_{det})	2.0×10^{-11} m/s Pa
Biofilm density (ρ_b)	2.0 kg/m ³
Maximum reaction rate (k)	1.6×10^{-3} 1/s
Half-saturation constant (K_s)	1.0×10^{-3} kg/m ³
Yield coefficient (Y)	0.5
Solute diffusivity in water (D_w)	1.0×10^{-9} m ² /s
Solute diffusivity in biofilm (D_b)	5.0×10^{-10} m ² /s
Pressure drop (Δp)	5.0 Pa
Inlet solute concentration (C_{in})	1.0×10^{-4} kg/m ³
Initial biofilm volume fraction (ϵ_{ini})	0.01

throats. This assumption corresponds to the scenario of discrete biomass distribution (i.e., microcolonies) (Taylor and Jaffe 1990). In case 2, we increased the pressure drop across the network by ten times, in order to highlight the non-equilibrium mass exchange of solute between water phase and biofilm. Case 3 and case 4 were selected for studying the condition that sufficient solute is available for bioreaction. To investigate the effect of distribution pattern of biofilm, in case 5, we assumed that biofilm was present in both pore bodies and pore throats. Solute can diffuse in biofilm throughout the whole network. In case 6, we considered permeable biofilm, in order to investigate the effect of biofilm permeability on its growth.

5 Results and Discussion

5.1 Model Verification

For the purpose of comparison, water pressure and solute concentrations were averaged over each pore body and each pore throat in the direct simulation. As shown in Fig. 6a, the pressure profile was very well modeled by the PN model. Figure 6b shows the distributions of normalized solute concentrations along the flow direction obtained from the two numerical methods. Solute concentrations in the water phase and biofilm are significantly different. This indicates that non-equilibrium mass exchange of solute prevailed in the computational domain. This was well modeled by the PN model. However, the PN model predicted slightly higher concentration in the water phase and slightly lower concentration in the biofilm. There are two reasons for the concentration discrepancies. First, it is because narrow regions in the direct simulation were approximated by cylindrical pore throats in the PN modeling. Second, in the formulation of the present pore-network model, local concentration variation in a pore element induces certain misestimation in calculating advective and diffusive fluxes. This is more pronounced under very high Damköhler and Péclet numbers. Nevertheless, this verification study shows that the PN model results are sufficiently reliable. It can be used for solute transport in porous media with biofilm, particularly under non-equilibrium conditions.

5.2 Case Studies

5.2.1 Flow Rate Effect (Case 1 and Case 2)

At any given time step, Eq. 1 was solved to obtain the pressure and flow fields. We calculated the network permeability K from

$$K = \mu \frac{Q_{\text{in}} L_x}{A_x \Delta p} \quad (13)$$

where Q_{in} is the water flux entering the network via the first row of pore throats at the inlet, A_x is the inlet area including the solid part, L_x is the length of the network in the flow direction, and Δp is the pressure drop across the network.

Obviously, as the biofilm growth and pore-geometry change, the network permeability decreases. Figure 7 shows the temporal evolutions of normalized permeability (K/K^0), with

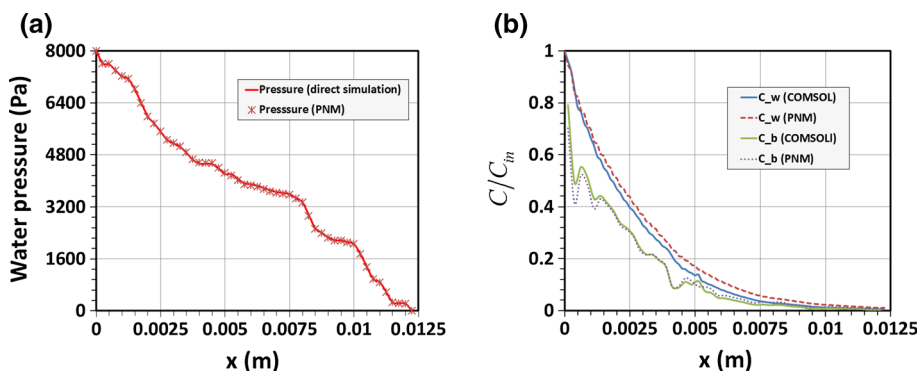


Fig. 6 Comparisons between the PN and direct simulations in terms of **a** pressure profile along the flow direction and **b** solute concentration distributions

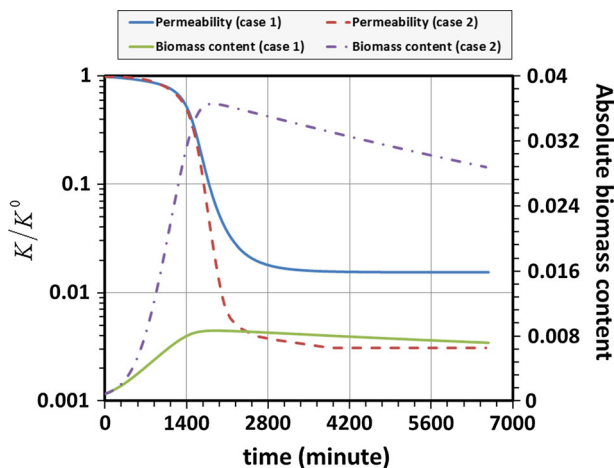


Fig. 7 Temporal evolutions of permeability and biomass content in the pore network in case 1 and case 2

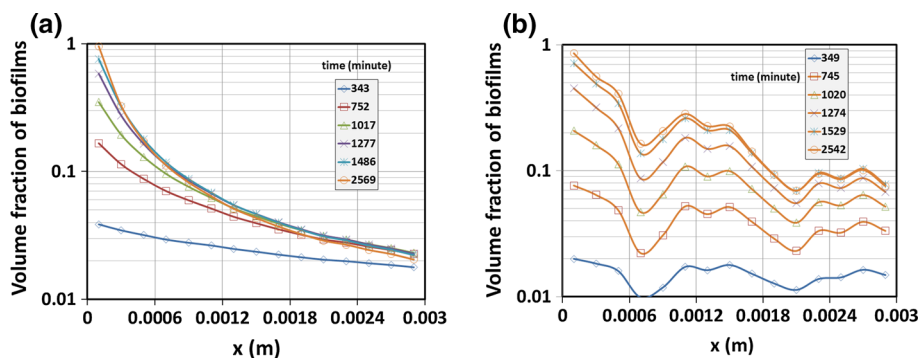


Fig. 8 Distributions of cross-sectional averaged biofilm volume fraction along the flow direction at different times in **a** case 1 and **b** case 2

K^0 being the initial permeability, and the absolute biomass content defined as the ratio of the volume of all biofilm in the network to the volume of the REV. It is evident that, in response to biofilm growth, the medium permeability in either case decreased first slowly, then sharply to a constant value. At higher flow rate (case 2), there is a larger reduction in permeability to the order of 10^{-3} . Comparing the temporal evolution of biomass content indicates that increasing flow rate gave rise to a much larger amount of biofilm in the network. In case 2, after reaching a peak, the biomass content started to decrease. This indicates that decay of biofilm started to play a dominant role in the regions away from the inlet part due to the solute mass transfer limitations. But, this decay did not significantly influence the evolution of permeability.

Figure 8 shows the distributions of cross-sectional averaged biofilm volume fraction along the flow direction at different times. Note that the average was done over cross sections where pore bodies are absent. In case 1, biofilm grew continuously with time close to the inlet. After 2569 min, severe clogging occurred at the inlet as shown in Fig. 8a. At the regions away from the inlet, no obvious growth of biofilm was observed mainly due to unavailability of nutrient. Increasing flow rate (case 2) considerably influenced the distribution of biofilm as shown

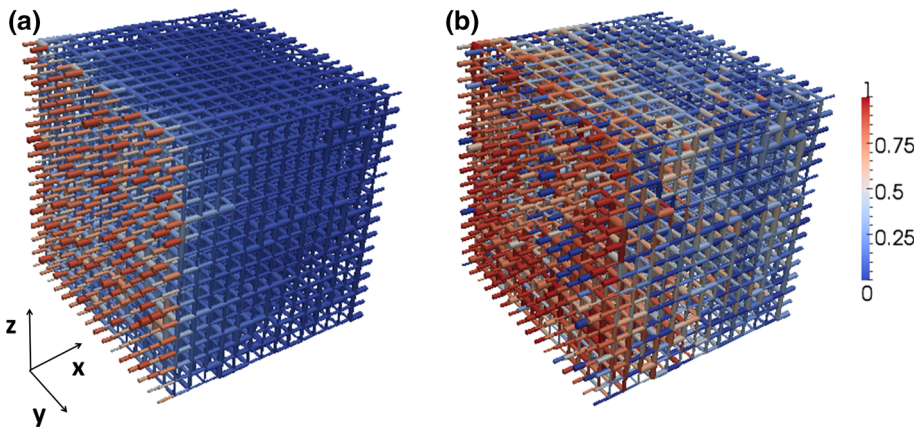
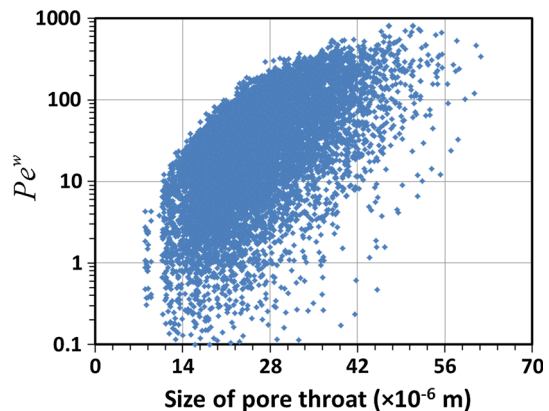


Fig. 9 Distributions of biofilm volume fraction in the pore network in **a** case 1 ($t = 1486$ min) and **b** case 2 ($t = 1529$ min)

Fig. 10 Distribution of Péclet number in case 2



in Fig. 8b. First, it is seen that the distributions were non-monotonic. Second, compared to the results in case 1, the inlet part in case 2 was less clogged even though more solute was available. This indicates that main flow paths with low flow rates were mostly clogged, whereas biofilm in pore throats with high flow rates was wiped by water shear force.

Figure 9 shows the detailed distributions of biofilm volume fraction in the pore network (note that pore bodies were not shown as they did not contain any biofilm). In case 1, the distribution was quite regular with very large volume fractions at the inlet and very small volume fractions away from the inlet. But, in case 2, the distribution was more complicated. It is seen that pore throats in the absence of biofilm existed throughout the network at $t = 1529$ min. They were primarily oriented in the flow direction. This indicates that increasing flow rate removed initially distributed biofilm in these throats at a very early stage when the water shear force was largest. As a result, no biofilm was available to support subsequent growth.

Figure 10 shows the logarithmic distribution of Péclet number for water flow at the initial stage of biofilm growth in case 2. Here, Péclet number was defined as $Pe^w = 2Q_{ij}/\pi r_{ij}^0(1 - \varepsilon^b)D_w$. Also, according to the definition of Damköhler number (see Sect. 3.4), the mean values of Péclet number and Damköhler number are around 100 and 20,

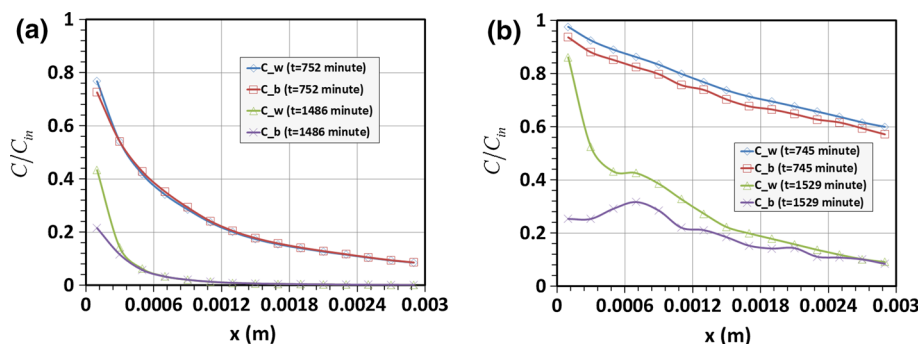


Fig. 11 Distributions of solute concentrations in the water phase and biofilm at different times in **a** case 1 and **b** case 2

respectively. Previous studies (Orgogozo et al. 2010) indicated that under such conditions, non-equilibrium mass exchange of solute between water phase and biofilm needed to be taken into account. This was checked by comparing distributions of normalized solute concentrations (C/C_{in}) in the water phase and biofilm at different times in case 1 and case 2. In case 1 (Fig. 11a), at early times ($t = 752$ min), local equilibrium was observed. But, at $t = 1486$ min, a significant difference in solute concentrations was found at the inlet region where the biofilm volume fraction was around 0.8. In case 2 (Fig. 11b), non-equilibrium was observed even at early times (where there was small biofilm volume fraction), and it became much stronger at large volume fractions of biofilm. It is concluded that high flow rate and large biofilm volume fraction both enhance non-equilibrium mass exchange of solute between water phase and biofilm. Finally, it is noted that, in this work, we employed a relatively large bioreaction rate, in order to highlight the non-equilibrium mass exchange of solute at a large Damköhler number. As a result, severe mass transfer limitation existed in the regions away from the inlet, and there only a small amount of biofilm was formed. Also, it can be expected that large Damköhler number and non-equilibrium condition prevail, when coarse porous medium like a pack of glass beads is under consideration (see Pintelon et al. 2012). In general, under the condition of solute transfer limitation, three parameters, namely Péclet number, Damköhler number, and biofilm volume fraction, together determine how far solute mass exchange is away from local equilibrium.

5.2.2 Inlet Concentration Effect (Case 3 and Case 4)

In case 3 and case 4, inlet solute concentrations of 1 kg/m^3 and 0.1 kg/m^3 , respectively, were specified. These are much larger than the inlet concentration in case 1 ($1.0 \times 10^{-4} \text{ kg/m}^3$) and also much larger than the half-saturation constant (0.001 kg/m^3). As a result, Monod kinetics reduced to zeroth-order reaction. So, Eq. 11 was used to prescribe the pore-scale mass exchange coefficient. Figure 12 shows the temporal evolutions of permeability and biomass content in the pore network. Compared to the results in case 1, medium permeability reduced to an extremely small value in a short time. Also, the temporal evolutions of biomass content in the two cases indicate that the whole network was severely clogged with biofilm.

Figure 13 shows the distributions of cross-sectional averaged volume fraction of biofilm at different times. It is seen that in case 3 (Fig. 13a), biofilm grew uniformly in the whole network. This is because sufficient solute was available during the whole process of biofilm

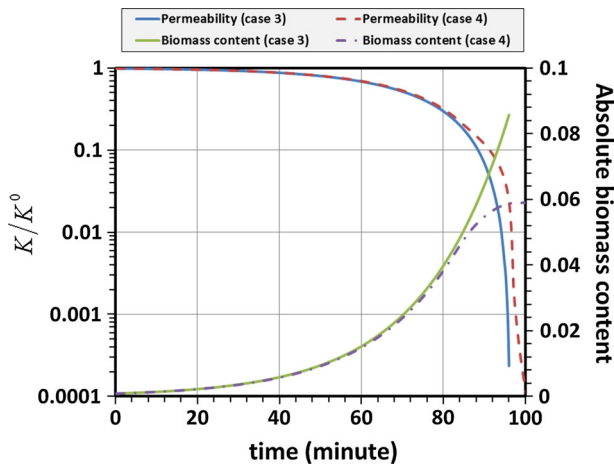


Fig. 12 Temporal evolutions of permeability and biomass content in the pore network in case 3 and case 4

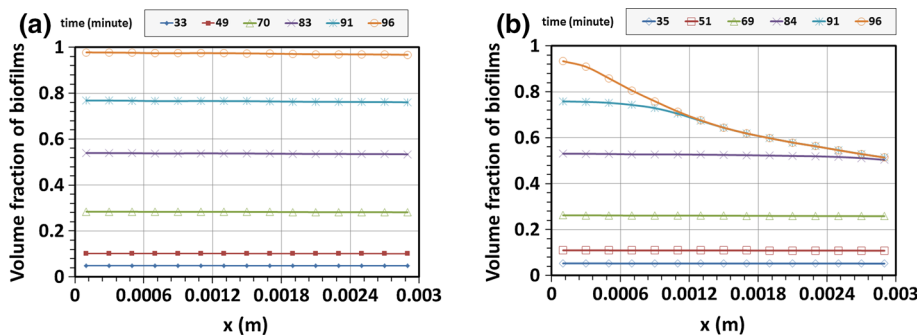


Fig. 13 Distributions of cross-sectional averaged volume fraction of biofilm along the flow direction at different times in **a** case 3 and **b** case 4

growth (i.e., no mass transfer limitation). In case 4 (Fig. 13b), biofilm first uniformly grew to the volume fraction of around 0.55; then, the growth rate of biofilm became smaller and smaller along the flow direction. This is because at large biofilm volume fraction, mass transfer limitation occurred in the regions away from the inlet. Figure 14 shows the distributions of solute concentrations in the water phase and biofilm at $t = 96$ min. We can see that in case 3, the outlet solute concentration was around 0.2 which was still quite high with respect to the half-saturation constant. But, in case 4, most solute was consumed at the inlet region. From Fig. 14, it is also seen that local-equilibrium mass transfer prevailed at high solute concentrations. In the modeling perspective, under such conditions, there is no need to track the solute mass exchange between water phase and biofilm. This can considerably simplify the numerical model. Finally, it is noted that in case 4, in the region away from the inlet, solute consumption experienced zeroth-order bioreaction before severe clogging occurred, and afterward first-order bioreaction because of the mass transfer limitation ($t > 91$ min). But, only Eq. 11 was used for calculating the mass exchange coefficient. This assumption will be released in a further study by including the solute concentration in the fitting of the mass exchange coefficient (see Qin and Hassanizadeh 2015).

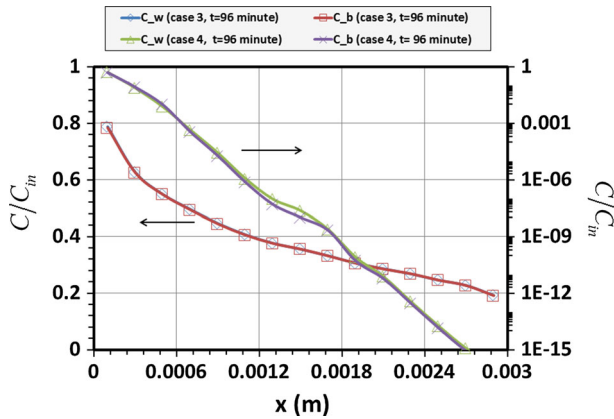


Fig. 14 Distributions of solute concentrations in the water phase and biofilm at $t=96$ min in case 3 (*left axis*) and case 4 (*right axis*)

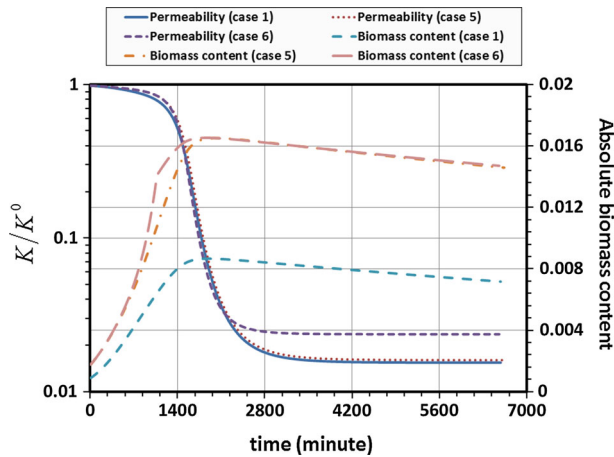


Fig. 15 Temporal evolutions of permeability and biomass content in the pore network in case 1, case 5, and case 6

5.2.3 Effects of Biofilm Morphology and Permeability (Case 5 and Case 6)

Figure 15 displays the temporal evolutions of permeability and biomass content in the pore network in case 1, case 5, and case 6. In cases 5 and 6, we assumed that the biofilm was also present in pore bodies. In case 6, nonzero permeability was assigned to the biofilm. Comparing case 1 and case 5 indicates that, under the operating condition given in Table 4, the assumption of continuous biofilm did not affect the temporal evolution of permeability. This is because here the permeability reduction was mainly caused by the clogging of pore throats near the inflow boundary. Also, as expected, the biomass content was approximately doubled in case 5. In case 6, governing equations for permeable biofilm given in Appendix 1 were solved with the value of parameter X set to be 1000 (Thullner and Baveye 2008). Comparing case 5 and case 6 indicates that considering permeable biofilm did not significantly influence the temporal evolution of permeability. But, as expected, at the end, a little higher

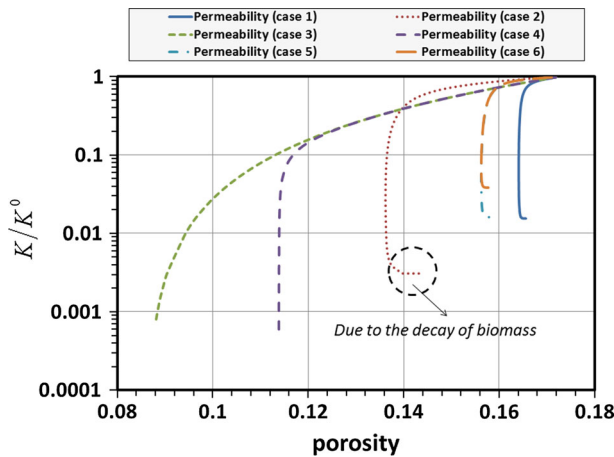


Fig. 16 Changes of medium permeability with the porosity of the pore network for all cases

permeability was observed in case 6. This is because biofilm also contributed to water flow in pore throats. At low volume fractions of biofilm (before 700 min), biofilm permeability had no influence on the temporal evolution of biomass content. This indicates that diffusion played a dominant role in transporting solute into the biofilm. After that, biofilm permeability started to enhance biofilm growth near the inlet part. It is worth noting that, if the mass exchange coefficient was overwhelmingly underestimated (Thullner and Baveye 2008), the effect of biofilm permeability would be exaggerated. With LB direct simulations, Pintelon et al. (2012) showed a significant influence of biofilm permeability on medium permeability and biomass content. This is because in their case, non-equilibrium condition was very strong, and advection was comparable to diffusion transport of solute into biofilm. Therefore, in further studies, it is important to identify under what conditions biofilm permeability needs to be taken into account.

5.2.4 Permeability Decrease with Porosity

Due to the clogging in the pore network by the biofilm, the water permeability decreased with the decrease in the porosity. The relationship between permeability and porosity serves as an important constitutive equation in macroscale modeling of biofilm (Ebigbo et al. 2010). The PN modeling is able to provide this information. The changes of permeability with the porosity of the pore network for all cases are shown in Fig. 16. It is seen that before a sudden drop of the permeability due to the clogging, the permeability decrease with porosity was similar in all cases. The point of a sudden drop in permeability was strongly dependent on biofilm morphology and operating conditions such as inlet solute concentration. Basically, under the condition of low inlet solute concentration (see cases 1, 5, and 6), the permeability decreased considerably with a very small decrease in porosity. As discussed before, this is because the reduction in permeability was mainly caused by the clogging of biofilm at the inlet, while much less biofilm was present in regions away from the inlet (see Fig. 8). But, under the condition of high inlet solute concentration (see case 3 or 4), the threshold was at a much lower porosity value. Finally, it was observed that increasing flow rate (case 2) would delay the reduction in the permeability.

6 Conclusions and Future Perspectives

In this work, we have developed a PN model for solute transport and biofilm growth in porous media. Compared to previous PN studies of biofilm growth, the present PN model holds two distinctive features. First, a structure of pore network was used in which pore bodies represent large pore spaces, while pore throats represent narrow regions connecting pore throats. In the modeling, we tracked solute concentrations in both pore bodies and pore throats. Second, a newly developed mass exchange term was implemented in the solute transport equations. Also, numerically fitted equations of mass exchange coefficient were provided. Based on a number of case studies with the PN model, we obtained the following main conclusions.

1. Under the condition of insufficient solute supply (case 1), biofilm clogging occurred at the inlet region. This resulted in the fast reduction in medium permeability. Increasing water flow rate (case 2) would increase biofilm accumulation in the regions away from the inlet. Meanwhile, a patchy-type distribution pattern of biofilm was obtained, mainly because of the detachment of biofilm in some pore throats.
2. Under the condition of sufficient solute supply (case 3), biofilm grew uniformly throughout the network.
3. At high Péclet and Damköhler numbers, non-equilibrium mass exchange of solute between water phase and biofilm needed to be accounted for, particularly at large biofilm volume fraction. But, equilibrium prevailed under the condition of sufficient solute supply.
4. Under the operating conditions used in this work, the PN model predicted that biofilm morphology had no significant influence on the temporal evolution of permeability. At low biofilm volume fractions, biofilm permeability had no influence on the temporal evolution of biomass content, because diffusion played a dominant role in transporting solute into the biofilm. After that, biofilm permeability started to enhance biofilm growth near the inlet part.
5. Finally, it was shown that no unique relationship between permeability and porosity was obtained. It was strongly dependent on biofilm morphology and operating conditions such as the availability of solute for bioreaction.

In future studies, the following issues need to be addressed. First, instead of a regular lattice-based pore network, an irregular one with a distribution of coordinate numbers will be generated stochastically or directly extracted from a porous medium of interest. Second, floating biomass in water phase should be accounted for. It can interact with immobile biofilm through attachment and detachment mechanisms. Finally, a more general equation of mass exchange coefficient needs to be fitted, in order to cover a broad range of operating conditions.

Acknowledgments This research was supported by the Dutch Technology Foundation STW, which is part of the Netherlands Organisation for Scientific Research (NOW) and which is partly funded by the Ministry of Economic Affairs.

Open Access This article is distributed under the terms of the Creative Commons Attribution 4.0 International License (<http://creativecommons.org/licenses/by/4.0/>), which permits unrestricted use, distribution, and reproduction in any medium, provided you give appropriate credit to the original author(s) and the source, provide a link to the Creative Commons license, and indicate if changes were made.

Appendix 1: Governing Equations for Permeable Biofilm

When permeable biofilm is considered, following the idea used by Dupin et al. (2001); Thullner and Baveye (2008), the mass conservation of water at pore body i is

$$\sum_j^{N_i} Q_{ij} = \sum_j^{N_i} \frac{\pi (r_{ij}^0)^4}{8\mu} \left[(1 - \varepsilon_{ij}^b)^2 + \frac{2\varepsilon_{ij}^b - (\varepsilon_{ij}^b)^2}{X} \right] \frac{(p_i - p_j)}{L_{ij}} = 0 \quad (14)$$

where Q_{ij} is the total water flux through cylindrical pore throat ij with biofilm attached around solid walls and X is a parameter controlling the effect of biomass on water flow in the biofilm. Once the pressure field is obtained, the water fluxes through the void space and biofilm can be, respectively, calculated by

$$Q_{ij}^w = \frac{\pi (r_{ij}^0)^4 (1 - \varepsilon_{ij}^b)^2}{8\mu} \left[1 + \frac{2\varepsilon_{ij}^b}{X (1 - \varepsilon_{ij}^b)} \right] \frac{(p_i - p_j)}{L_{ij}} \quad (15)$$

$$Q_{ij}^b = \frac{\pi (r_{ij}^0)^4 (\varepsilon_{ij}^b)^2}{8\mu} \frac{(p_i - p_j)}{L_{ij}} \quad (16)$$

The mass conservations of solute in water phase and biofilm at pore body i are given, respectively,

$$V_i^0 \varepsilon_i^w \frac{dC_i^w}{dt} = -C_i^w \sum_j^{N_i} \max(Q_{ij}^w, 0) - \sum_j^{N_i} C_{ij}^w \min(Q_{ij}^w, 0) - \sum_j^{N_i} D_{ij}^w A_{ij}^w \frac{C_i^w - C_{ij}^w}{L_{ij}/2} - V_i^0 \frac{D_w D_b}{D_w + D_b} \gamma_i \xi_i (C_i^w - C_i^b) \quad (17)$$

$$V_i^0 \varepsilon_i^b \frac{dC_i^b}{dt} = -C_i^b \sum_j^{N_i} \max(Q_{ij}^b, 0) - \sum_j^{N_i} C_{ij}^b \min(Q_{ij}^b, 0) - \sum_j^{N_i} D_{ij}^b A_{ij}^b \frac{C_i^b - C_{ij}^b}{L_{ij}/2} + V_i^0 \frac{D_w D_b}{D_w + D_b} \gamma_i \xi_i (C_i^w - C_i^b) - V_i^0 \varepsilon_i^b k \frac{C_i^b}{K_s + C_i^b} \rho_b \quad (18)$$

Likewise, the mass conservations of solute in water phase and biofilm at pore throat ij are given, respectively,

$$V_{ij}^0 \varepsilon_{ij}^w \frac{dC_{ij}^w}{dt} = (C_i^w - C_{ij}^w) \max(Q_{ij}^w, 0) + (C_{ij}^w - C_j^w) \min(Q_{ij}^w, 0) + D_{ij}^w A_{ij}^w \frac{C_i^w - C_{ij}^w}{L_{ij}/2} + D_{ij}^w A_{ij}^w \frac{C_j^w - C_{ij}^w}{L_{ij}/2} - V_{ij}^0 \frac{D_w D_b}{D_w + D_b} \gamma_{ij} \xi_{ij} (C_{ij}^w - C_{ij}^b) \quad (19)$$

$$V_{ij}^0 \varepsilon_{ij}^b \frac{dC_{ij}^b}{dt} = (C_i^b - C_{ij}^b) \max(Q_{ij}^b, 0) + (C_{ij}^b - C_j^b) \min(Q_{ij}^b, 0) + D_{ij}^b A_{ij}^b \frac{C_i^b - C_{ij}^b}{L_{ij}} + D_{ij}^b A_{ij}^b \frac{C_j^b - C_{ij}^b}{L_{ij}} + V_{ij}^0 \frac{D_w D_b}{D_w + D_b} \gamma_{ij} \xi_{ij} (C_{ij}^w - C_{ij}^b) - k \frac{C_{ij}^b}{K_s + C_{ij}^b} \rho_b V_{ij}^0 \varepsilon_{ij}^b \quad (20)$$

Finally, with proper boundary conditions, Eqs. (14–20, 6–7) together with closure equations provided in Sects. 3.2 and 3.3 can be solved for flow field, solute concentrations, and biofilm volume fractions in the pore network.

Appendix 2: Numerical Scheme for Solving Transport Equations of a General Reactive Solute in a Pore Network

As to a general reactive solute, first, its mass conservation in pore body i is

$$V_i \frac{dC_i}{dt} = -C_i \sum_j \max(Q_{ij}, 0) - \sum_j C_{ij} \min(Q_{ij}, 0) - \sum_j D_{ij} A_{ij} \frac{C_i - C_{ij}}{L_{ij}/2} + (S_i^1 + S_i^2 C_i) V_i \quad (21)$$

The last term on the r.h.s. represents a general sink/source term. Then, Eq. 21 can be implicitly discretized as

$$C_i^{t+\Delta t} = -M_i C_i^{t+\Delta t} \sum_j \max(Q_{ij}, 0) - M_i \sum_j C_{ij}^{t+\Delta t} \min(Q_{ij}, 0) - M_i \sum_j B_{ij} (C_i^{t+\Delta t} - C_{ij}^{t+\Delta t}) + (S_i^1 + S_i^2 C_i^{t+\Delta t}) \Delta t + C_i^t \quad (22)$$

where Δt is the time step, the superscripts $t + \Delta t$ and t denote that the referred quantities are evaluated at current and previous time steps, respectively, $M_i = \Delta t/V_i$, and $B_{ij} = 2D_{ij}A_{ij}/L_{ij}$.

The mass conservation of solute in pore throat ij is

$$V_{ij} \frac{dC_{ij}}{dt} = (C_i - C_{ij}) \max(Q_{ij}, 0) + (C_{ij} - C_j) \min(Q_{ij}, 0) + B_{ij} (C_i - C_{ij}) + B_{ij} (C_j - C_{ij}) + (S_{ij}^1 + S_{ij}^2 C_{ij}) V_{ij} \quad (23)$$

where the last term on the r.h.s. represents a general sink/source term. Also, we implicitly discretize Eq. 23 to be the form

$$C_{ij}^{t+\Delta t} = N_{ij} (C_i^{t+\Delta t} - C_{ij}^{t+\Delta t}) \max(Q_{ij}, 0) + N_{ij} (C_{ij}^{t+\Delta t} - C_j^{t+\Delta t}) \min(Q_{ij}, 0) + N_{ij} B_{ij} (C_i^{t+\Delta t} - C_{ij}^{t+\Delta t}) + N_{ij} B_{ij} (C_j^{t+\Delta t} - C_{ij}^{t+\Delta t}) + (S_{ij}^1 + S_{ij}^2 C_{ij}^{t+\Delta t}) \Delta t + C_{ij}^t \quad (24)$$

where $N_{ij} = \Delta t / V_{ij}$. For the substitution of Eqs. 24 into 22 to eliminate $C_i^{t+\Delta t}$, we obtain the following discretized equation for solute concentrations in pore bodies:

$$\begin{aligned} & \left[1 + M_i \sum_j \max(Q_{ij}, 0) + M_i \sum_j B_{ij} - S_i^2 \Delta t \right. \\ & \quad \left. - M_i \sum_j \frac{N_{ij} B_{ij} (B_{ij} + |Q_{ij}|)}{1 + N_{ij} |Q_{ij}| + 2N_{ij} B_{ij} - S_{ij}^2 \Delta t} \right] C_i^{t+\Delta t} \\ & = \left[M_i \sum_j \frac{N_{ij} (B_{ij} - \min(Q_{ij}, 0))^2}{1 + N_{ij} |Q_{ij}| + 2N_{ij} B_{ij} - S_{ij}^2 \Delta t} \right] C_j^{t+\Delta t} + C_i^t + S_i^1 \Delta t \\ & \quad + M_i \sum_j \frac{(B_{ij} - \min(Q_{ij}, 0)) (S_{ij}^1 \Delta t + C_{ij}^t)}{1 + N_{ij} |Q_{ij}| + 2N_{ij} B_{ij} - S_{ij}^2 \Delta t} \end{aligned} \quad (25)$$

Finally, with proper boundary conditions for inlet and outlet pore bodies, we solve for solute concentrations in all pore bodies. Once $C_i^{t+\Delta t}$ is obtained, $C_j^{t+\Delta t}$ can be calculated from Eq. 24.

References

- Afrapoli, M.S., Alipour, S., Torsaeter, O.: Fundamental study of pore scale mechanisms in microbial improved oil recovery processes. *Transp. Porous Media* **90**, 949–964 (2011)
- Al-Kharusi, A.S., Blunt, M.J.: Network extraction from sandstone and carbonate pore space images. *J. Pet. Sci. Technol.* **56**, 219–231 (2007)
- Aris, R.: On the dispersion of a solute in a fluid flowing through a tube. *Proc. R. Soc. Lond. A* (1956). doi:[10.1098/rspa.1956.0065](https://doi.org/10.1098/rspa.1956.0065)
- Baveye, P., Valocchi, A.: An evaluation of mathematical models of the transport of biologically reacting solutes in saturated soils and aquifers. *Water Resour. Res.* **25**, 1413–1421 (1989)
- Baveye, P., Vandevivere, P., Hoyle, B.L., DeLeo, P.C., Sanchez de Lozada D.: Environmental impact and mechanisms of the biological clogging of saturated soils and aquifer materials. *Crit. Rev. Environ. Sci. Technol.* **28**, 123–191 (1998)
- Blunt, M.J.: Flow in porous media-pore-network models and multiphase flow. *Curr. Opin. Colloid Interface Sci.* **6**, 197–207 (2001)
- Boltz, J.P., Morgenroth, E., Sen, D.: Mathematical modeling of biofilms and biofilm reactors for engineering design. *Water Sci. Technol.* **62**, 1821–36 (2010)
- Bottero, S., Storck, T., Heimovaara, T.J., van Loosdrecht, M.C.M., Enzien, M.V., Picioreanu, C.: Biofilm development and the dynamics of preferential flow paths in porous media. *Biofouling* **29**, 1069–1086 (2013)
- Budek, A., Szymczak, P.: Network models of dissolution of porous media. *Phys. Rev. E* **86**, 056318 (2012)
- Cherblanc, F., Ahmadi, A., Quintard, M.: Two-domain description of solute transport in heterogeneous porous media: comparison between theoretical predictions and numerical experiments. *Adv. Water Resour.* **30**, 1127–1143 (2007)
- Cunningham, A.B., Characklis, W.G., Abedeen, F., Crawford, D.: Influence of biofilm accumulation on porous media hydrodynamics. *Environ. Sci. Technol.* **25**, 1305–1311 (1991)
- Cunningham, J.A., Mendoza-Sanchez, I.: Equivalence of two models for biodegradation during contaminant transport in groundwater. *Water Resour. Res.* **42**, W02416 (2006)
- Chambless, J.D., Steward, P.S.: A three-dimensional computer model analysis of three hypothetical biofilm detachment mechanisms. *Biotechnol. Bioeng.* **97**, 1573–1584 (2007)
- Dunsmore, B.C., Bass, C.J., Lappin-Scott, H.M.: A novel approach to investigate biofilm accumulation and bacterial transport in porous matrices. *Environ. Microbiol.* **6**, 183–187 (2004)
- Davit, Y., Debenest, G., Wood, B.D., Quintard, M.: Modeling non-equilibrium mass transport in biologically reactive porous media. *Adv. Water Resour.* **33**, 1075–1093 (2010)

- Dillon, R., Fauci, L.: A microscale model of bacterial and biofilm dynamics in porous media. *Biotechnol. Bioeng.* **68**, 536–547 (2000)
- Dykaar, B., Kitanidis, P.K.: Macrotransport of a biologically reacting solute through porous media. *Water Resour. Res.* **32**, 307–320 (1996)
- Dupin, H.J., Kitanidis, P.K., McCarty, P.L.: Simulations of two-dimensional modeling of biomass aggregate growth in network models. *Water Resour. Res.* **37**, 2981–2994 (2001)
- Ebigbo, A., Helmig, R., Cunningham, A.B., Class, H., Gerlach, R.: Modelling biofilm growth in the presence of carbon dioxide and water flow in the subsurface. *Adv. Water Resour.* **33**, 762–781 (2010)
- Ebigbo, A., Phillips, A., Gerlach, R., Helmig, R., Cunningham, A.B., Class, H., Spangler, L.H.: Darcy-scale modeling of microbially induced carbonate mineral precipitation in sand columns. *Water Resour. Res.* **48**, W07519 (2012)
- Ezeuko, C.C., Sen, A., Grigoryan, A., Gates, I.D.: Pore-network modeling of biofilm evolution in porous media. *Biotechnol. Bioeng.* **108**, 2413–2423 (2011)
- Graf von der Schulenburg, D.A., Pintelon, T.R.R., Picioreanu, C., Van Loosdrecht, M.C.M., Johns, M.L.: Three-dimensional simulations of biofilm growth in porous media. *AIChE J.* **55**, 494–504 (2009)
- Golfier, F., Wood, B.D., Orgogozo, L., Quintard, M., Bues, M.: Biofilm in porous media: development of macroscopic transport equations via volume averaging with closure for local mass equilibrium conditions. *Adv. Water Resour.* **32**, 463–485 (2009)
- Iltis, G.C., Armstrong, R.T., Jansik, D.P., Wood, B.D., Wildenschild, D.: Imaging biofilm architecture within porous media using synchrotron-based X-ray computed microtomography. *Water Resour. Res.* **47**, W02601 (2011)
- Jiang, Z., van Dijke, M.I.J., Wu, K., Couples, G.D., Sorbie, K.S., Ma, J.: Stochastic pore network generation from 3D rock images. *Transp. Porous Med.* **94**, 571–593 (2012)
- Kapellos, G.E., Alexiou, T.S., Payatakes, A.C.: Hierarchical simulator of biofilm growth and dynamics in granular porous materials. *Adv. Water Resour.* **30**, 1648–1667 (2007)
- Kim, S., Corapcioglu, M.Y.: The role of biofilm growth in bacteria-facilitated contaminant transport in porous media. *Transp. Porous Media* **26**, 161–181 (1997)
- Kim, D.S., Fogler, H.S.: Biomass evolution in porous media and its effect on permeability under starvation conditions. *Biotechnol. Bioeng.* **69**, 47–56 (2000)
- Li, L., Peters, C.A., Celia, M.A.: Upscaling geochemical reaction rates using pore-scale network modeling. *Adv. Water Resour.* **29**, 1351–1370 (2006)
- MarDonald, T.R., Kitanidis, P.K., McCarty, P.L., Roberts, P.V.: Mass-transfer limitations for macroscale bioremediation modeling and implications on aquifer clogging. *Ground Water* **37**, 523–531 (1999)
- Mitchell, A.C., Phillips, A.J., Hiebert, R., Gerlach, R., Spangler, L.H., Cunningham, A.B.: Biofilm enhanced geologic sequestration of supercritical CO₂. *Int. J. Greenh. Gas Control* **3**, 90–99 (2009)
- Orgogozo, L., Golfier, F., Bues, M., Quintard, M.: Upscaling of transport processes in porous media with biofilms in non-equilibrium conditions. *Adv. Water Resour.* **33**, 585–600 (2010)
- Pintelon, T.R.R., Graf von der Schulenburg, D.A., Johns, M.L.: Towards optimum permeability reduction in porous media using biofilm growth simulations. *Biotechnol. Bioeng.* **103**, 767–779 (2009)
- Pintelon, T.R.R., Picioreanu, C., van Loosdrecht, M.C.M.: The effect of biofilm permeability on bio-clogging of porous media. *Biotechnol. Bioeng.* **109**, 1031–1042 (2012)
- Potekhina, J.S., Sherisheva, N.G., Povetkina, L.P., Pospelov, A.P., Rakitina, T.A., Warnecke, F., Gottschalk, G.: Role of microorganisms in corrosion inhibition of metals in aquatic habitats. *Appl. Microbial. Biotechnol.* **52**, 639–646 (1999)
- Qin, C.Z., Hassanizadeh, S.M.: 2014 Solute mass exchange between water phase and biofilm for a single pore. *Transp. Porous Media* **109**, 255–278 (2015)
- Raouf, A., Hassanizadeh, S.M.: A new method for generating pore-network models of porous media. *Transp. Porous Media* **81**, 391–407 (2010)
- Raouf, A., Nick, H.M., Wolterbeek, T.K.T., Spiers, C.J.: Pore-scale modeling of reactive transport in wellbore cement under CO₂ storage conditions. *Int. J. Greenh. Gas Control* **11**, s67–s77 (2012)
- Rittmann, B.E.: The significance of biofilms in porous media. *Water Resour. Res.* **29**, 2195–2202 (1993)
- Rosenzweig, R., Shavit, U., Furman, A.: The influence of biofilm spatial distribution scenarios on hydraulic conductivity of unsaturated soils. *Vadose Zone J.* **8**, 1080–1084 (2009)
- Stewart, T.L., Kim, D.S.: Modeling of biomass-plug development and propagation in porous media. *Biochem. Eng. J.* **17**, 107–119 (2004)
- Suchomel, B.J., Chen, B., Allen, M.B.: Network model of flow, transport and biofilm effects in porous media. *Transp. Porous Media* **30**, 1–23 (1998a)
- Suchomel, B.J., Chen, B., Allen, M.B.: Macroscale properties of porous media from a network model of biofilm processes. *Transp. Porous Media* **31**, 39–66 (1998b)

- Taylor, S.W., Jaffe, P.R.: Substrate and biomass transport in a porous medium. *Water Resour. Res.* **26**, 2181–2194 (1990)
- Taylor, S.W., Milly, P.C.D., Jaffe, P.R.: Biofilm growth and the related changes in the physical properties of a porous medium: 2. permeability. *Water Resour. Res.* **26**, 2161–2169 (1990)
- Thullner, M., Baveye, P.: Computational pore network modeling of the influence of biofilm permeability on bioclogging in porous media. *Biotechnol. Bioeng.* **99**, 1337–1351 (2008)
- Thullner, M., Zeyer, J., Kinzelbach, W.: Influence of microbial growth on hydraulic properties of pore networks. *Transp. Porous Media* **49**, 99–122 (2002)
- Vandevivere, P., Baveye, P., Sanchez de Lozada, D., DeLeo, P.: Microbial clogging of saturated soils and aquifer materials: evaluation of mathematical models. *Water Resour. Res.* **31**, 2173–2180 (1995)
- Videla, H.A., Herrera, L.K.: Understanding microbial inhibition of corrosion: a comprehensive overview. *Int. Biodeterior. Biodegrad.* **63**, 896–900 (2009)
- Van Noorden, T.L., Pop, I.S., Ebigo, A., Helmig, R.: An upscaled model for biofilm growth in a thin strip. *Water Resour. Res.* **46**, W06505 (2010)
- Xu, Z.J., Meakin, P., Tartakovsky, A., Scheibe, T.D.: Dissipative-particle-dynamics model of biofilm growth. *Phys. Rev. E* **83**, 066702 (2011)
- Zysset, A., Stauffer, F., Dracos, T.: Modeling of reactive groundwater transport governed by biodegradation. *Water Resour. Res.* **30**, 2423–2434 (1994)
- Zuo, R.J.: Biofilms: strategies for metal corrosion inhibition employing microorganisms. *Appl. Microbial. Biotechnol.* **76**, 1245–1253 (2007)